



RESEARCH ARTICLE | NOVEMBER 23 2015

Computational analysis of metallic nanowire-elastomer nanocomposite based strain sensors

Sangryun Lee; Morteza Amjadi ; Nicola Pugno; Inkyu Park; Seunghwa Ryu 



AIP Advances 5, 117233 (2015)
<https://doi.org/10.1063/1.4936635>



CrossMark

AIP Advances

Why Publish With Us?



25 DAYS
average time
to 1st decision



740+ DOWNLOADS
average per article



INCLUSIVE
scope

[Learn More](#)



Computational analysis of metallic nanowire-elastomer nanocomposite based strain sensors

Sangryun Lee,¹ Morteza Amjadi,¹ Nicola Pugno,^{2,3,4} Inkyu Park,^{1,a} and Seunghwa Ryu^{1,b}

¹Department of Mechanical Engineering, Korea Advanced Institute of Science and Technology (KAIST), 291 Daehak-ro, Yuseong-gu, Daejeon 305-701, Republic of Korea

²Department of Civil, Environmental, and Mechanical Engineering, University of Trento, via Sommarive 14, I-38050 Provo (Trento), Italy

³Center for Materials and Microsystems, Fondazione Bruno Kessler, via Sommarive 18, I-38123 Provo (Trento), Trento, Italy

⁴School of Engineering and Materials Science, Queen Mary University of London, Mile End Road, E1 4NS London, United Kingdom

(Received 6 October 2015; accepted 12 November 2015; published online 23 November 2015)

Possessing a strong piezoresistivity, nanocomposites of metal nanowires and elastomer have been studied extensively for its use in highly flexible, stretchable, and sensitive sensors. In this work, we analyze the working mechanism and performance of a nanocomposite based stretchable strain sensor by calculating the conductivity of the nanowire percolation network as a function of strain. We reveal that the nonlinear piezoresistivity is attributed to the topological change of percolation network, which leads to a bottleneck in the electric path. We find that, due to enhanced percolation, the linearity of the sensor improves with increasing aspect ratio or volume fraction of the nanowires at the expense of decreasing gauge factor. In addition, we show that a wide range of gauge factors (from negative to positive) can be obtained by changing the orientation distribution of nanowires. Our study suggests a way to intelligently design nanocomposite-based piezoresistive sensors for flexible and wearable devices. © 2015 Author(s). All article content, except where otherwise noted, is licensed under a Creative Commons Attribution 3.0 Unported License. [<http://dx.doi.org/10.1063/1.4936635>]

INTRODUCTION

The demand for flexible and wearable strain sensors is increasing for various potential applications including personal health monitoring,¹ structural health monitoring,² and human motion capture for entertainment systems.^{3–5} The key characteristics of such devices including high flexibility, stretchability, and sensitivity cannot be satisfied by conventional strain gauges due to their poor stretchability and low sensitivity (maximum strain of 5% and gauge factor of ~ 2).^{3,6–8} In order to overcome the drawbacks of conventional sensors, several alternative sensors based on nanomaterial-elastomer nanocomposites such as metallic nanowire-polymer, carbon allotrope-polymer and metal nanoparticle-polymer have been studied.^{9–13} Carbon allotrope (such as graphene and carbon nanotube) based sensors have been investigated extensively because of their superior mechanical and electrical properties.^{14–17} Metallic nanowire-polymer nanocomposites have shown potential for use at high strain ranges.^{18–21}

Recently, we have developed a strain sensor based on silver nanowire-elastomer nanocomposites, which simultaneously possess high stretchability and high sensitivity.²² A sandwich structured design (silver nanowire thin film embedded between two layers of polydimethylsiloxane (PDMS)) was found to prevent the buckling/wrinkling of the silver nanowire thin films, ensuring a high reliability upon

^aCorresponding author E-mail: inkyu.park@kaist.ac.kr

^bCorresponding author E-mail: ryush@kaist.ac.kr

cyclic loading.²² Our sensors have shown excellent performance, with high linearity up to a strain of 40%; they also possess strong piezoresistivity with tunable gauge factors in the range of 2-14 with nanowire volume fraction. In addition, silver nanowire-polymer nanocomposites have successfully been employed for the development of stretchable, foldable, and transparent electrodes,^{8,23,24} flexible sensors^{25,26} and actuators,^{18,22,27} fuel cells^{28,29} and flexible thin film heaters.³⁰⁻³² However, the working mechanism of these strain sensors and electrodes is as yet unclear, largely due to the difficulties and limitations associated with real-time imaging of the microstructure. The main challenge, therefore, is the morphological tracking of the microstructure of the nanocomposite under external loads.

To address this, we have developed a new computational model based on a three dimensional (3D) resistor network to further uncover the primary mechanism involved in the strain-dependent behavior of the metal nanowire-elastomer based strain sensors and to suggest some possible key factors for performance improvement. We treat the metallic nanowires as rigid elements,⁸ because metal nanowire has much higher Young's modulus than those of elastomers.^{33,34} The re-orientation and re-positioning of metal nanowires inside the elastomeric matrix were assumed to be rigid body motion. With this assumption, our simulation revealed realistic and quantitative results that can explain the piezoresistive behavior of the metal nanowire-elastomer nanocomposites.²²

In this work, we conducted a computational analysis of metal nanowire-elastomer nanocomposite based stretchable strain sensors to further study the effects of nanowire volume fraction, aspect ratio, and orientation distribution on their performances. Also, the effect of contact resistance is discussed. We analyzed the evolution of a nanowire percolation network under different levels of strain and obtained the piezoresistive responses by calculating the resistance of a 3D resistor network. We show that the linear piezoresistive response at small strain levels originates from the expansion of the homogeneous percolation network, while the nonlinear response at high strain stems from the formation of bottle-necks in the nanowire network. Reduction of nanowire volume fraction increases the gauge factor, but reduces the strain range of linear responses simultaneously. Given the same volume fraction, the gauge factor increases with decreasing aspect ratio, while the linear regime decreases. We also found that the gauge factor can be tuned widely from a positive value to a negative value by changing the initial nanowire orientations, suggesting the feasibility of highly stretchable electrodes with minimal piezoresistivity. Although we conducted the simulation for particular material combination – silver nanowire and PDMS, the same trends can be valid for general metal nanowire-elastomer nanocomposites in which stiffer nanowires can be treated as rigid bodies. Our study provides a guideline to tune the piezoresistive response to design highly stretchable and flexible strain sensors and electrodes.

RESULTS AND DISCUSSION

We construct a 3D network model by randomly assigning the center of mass positions of the nanowires in the elastomer matrix, as depicted in Fig. 1(a). The alignment of nanowires is modeled by placing a pair of two points, P1 and P2, according to the given distribution of the angles θ and φ in the spherical coordinates (Fig. 1(b)). For simplicity, we assume that the two ends of the nanowires terminate in half spheres; we calculate the distance between nanowires using the analytic expression for the distance of two line segments. In order to clearly illustrate the effect of aspect ratio, we assign an identical aspect ratio to all the nanowires in one simulation cell. A resistor network is constructed by junction identification using inter-nanowire distances as the criterion; the resistance of the network is calculated by using Ohm's law.

We classify the junctions between the nanowire pairs into three categories: (i) complete contact with no contact resistance, (ii) tunneling junction with a certain cutoff resistance, and (iii) complete disconnection. If the distance d between a nanowire pair is shorter than the nanowire's diameter D , the pair is considered to be completely connected with no contact resistance. Thus, unphysical overlap between nanowires is allowed in our simulations, the effect of overlap between nanowires on the piezoresistivity is known to be negligible when the aspect ratio is high and the volume fraction is low.³⁵ We calculate the piezoresistivity with and without nonzero contact resistance for complete contact junctions, and find that the gauge factor is indeed almost identical for both cases. The tunneling

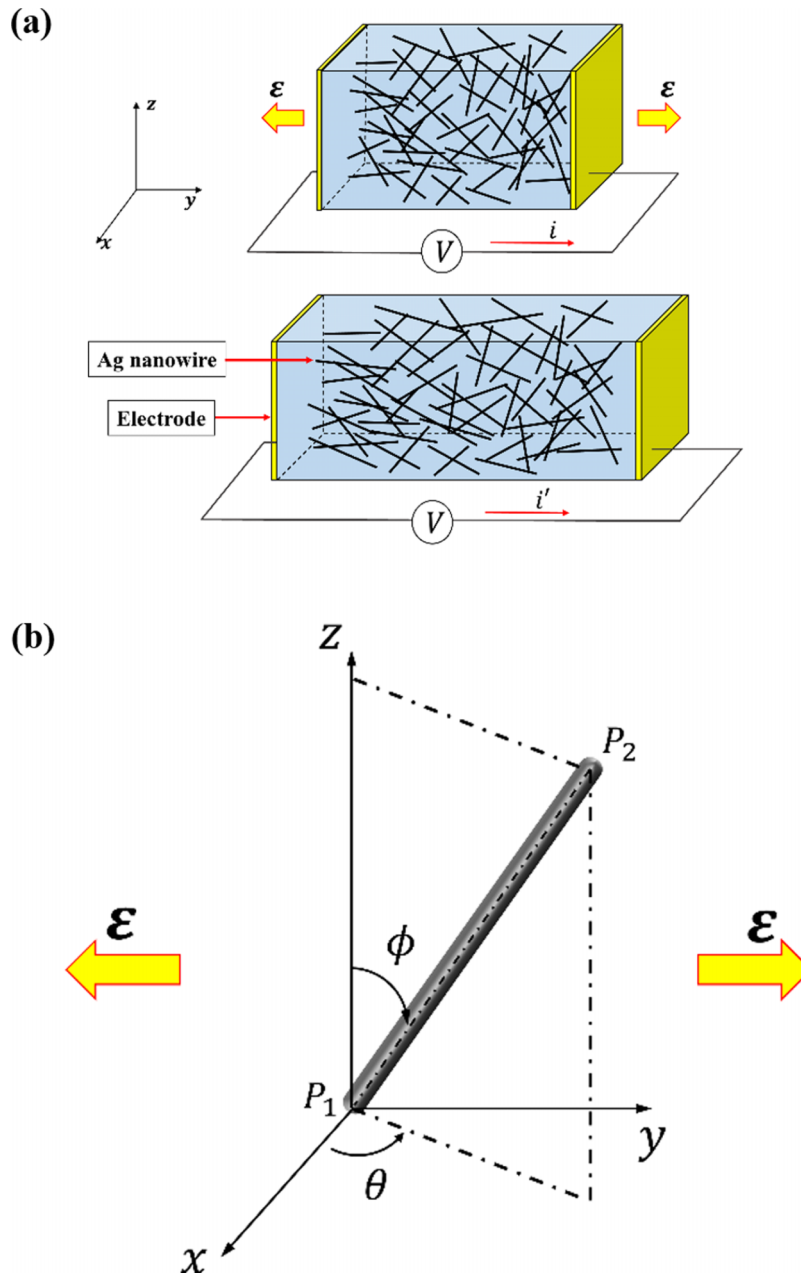


FIG. 1. (a) The schematic of the simulation; nanowires are randomly located inside the elastomer matrix. (b) The coordinate system used in this work.

contact is in effect when d is larger than D , but smaller than a cutoff distance D_c . To include current paths via quantum conductive junctions, the tunneling resistance between two neighboring nanowires can be approximated as^{36,37}

$$R_{\text{Tunnel}} = \frac{V}{AJ} = \frac{h^2 d}{Ae^2 \sqrt{2m\lambda}} \exp\left(\frac{4\pi d}{h} \sqrt{2m\lambda}\right), \quad (1)$$

where V is the electrical potential, e is the single electron charge, J is the tunneling current volume fraction, h is the Planck's constant, d is the distance between nanowires, λ is the height of the energy barrier (1 eV for PDMS), and A is the cross-section area of the tunnel. The distance D_c at which the tunneling resistance becomes 30 times larger than the resistance of a single nanowire is used as the

cutoff distance. The conductance does not change significantly with larger D_c , which implies that a large enough D_c has been chosen for our simulation. A nanowire pair with $d > D_c$ is classified as being disconnected; such pairs are not counted in constructing the 3D resistor model.

Because the elastic moduli of metal nanowires are much higher than those of elastomers, we model the re-position and re-orientation of the nanowires under strain as an affine transformation.³⁸ To compute the piezoresistive response, the resistance of the network is analyzed at every applied strain. We obtain a connectivity graph of the nanowires via the depth first search algorithm, and identify the percolation network connecting left and right ends of the simulation cell. We compute the resistance by determining the current flowing through the percolation network at a given voltage difference between both ends. Identification of the percolation network is important to speed up the calculation because it can allow us to avoid a pseudo-inverse calculation for a singular problem. Because the actual size of the elastomer in the experiments is beyond the computational capability, we apply a periodic boundary condition along the x and z axes to reduce the artifact that arises from the small simulation cell size ($[L_x, L_y, L_z] = [62.5\mu m, 60\mu m, 15\mu m]$).

We first compute the conductivity as a function of the nanowire volume fraction ϕ and compare this value with the conductance predicted using the analytic equation,

$$\sigma = \sigma_o(\phi - \phi_c)^t \quad (2)$$

where ϕ_c is the percolation threshold volume fraction, and σ_o, t are the fitting parameters. To compare our results with those from the existing theoretical models, we consider a bulk nanocomposite with a fully random orientation distribution of nanowires. Assuming slender rod geometry and fully random distribution, the threshold for the nanowires is given as

$$\phi_c = \frac{\pi R^2 L}{8\pi R^2 L + \pi L^2 R} = \frac{1}{8 + (AR)}, \quad (3)$$

where R, L, and AR are the radius, length, and aspect ratio of nanowires.^{39–42} The simulation results are fitted well with the theoretical prediction, as can be seen in Figure 2(a). The exponents t from the simulations are 105 and 3.2 for the aspect ratios of 65 and 2.8, respectively, which is larger than the universal value, 2, predicted by the percolation theory.⁴³ This difference may be attributed to the tunneling effect, which has not been considered in theoretical models.^{43,44} The theory predicts that the percolation threshold ϕ_c monotonically decreases as the aspect ratio increases, which means that higher aspect ratio nanowires are more effective in forming the percolation networks. As predicted by the theory, the conductance increases as the aspect ratio increases when the volume fraction is kept constant. Likewise, given the same aspect ratio, the conductance increases as the volume fraction increases because a denser percolation network is formed.

To reveal the origin of piezoresistivity, we compute the resistance of the percolation network at different strains. We perform a simulation with an incremental engineering strain of $\epsilon=0.05$ up to $\epsilon=1$, which is comparable to the maximum strain used in the experiment.^{18,22} Because of the small cell volume for simulation, the piezoresistive responses vary every time we begin from a different initial nanowire distribution. We average ten independent simulation results and present the resistivity versus strain curves in Fig. 2(b)-2(c), with error bars representing the standard deviations of the resistances at the given strains.

We find that a higher gauge factor is obtained at the expense of linearity when the volume fraction is lowered and vice versa, which agrees well with the experimental results.^{16,22,35} The sensor with small nanowire volume fraction can be used for the applications requiring high gauge factor with low strain; the high volume fraction sensor is the proper choice when high strain with acceptable gauge factor is needed. For example, low volume fraction strain sensors with high sensitivity can be employed for the measurement of very small movements of the human skin such as those involved in breathing and heartbeat. On the contrary, highly stretchable and linear strain sensors made of a high volume fraction network with acceptable gauge factors can be attached to the body for monitoring of large strains such as those induced by the bending of arm or knee joints.

The piezoresistive response also turns out to be highly dependent on the aspect ratio of nanowires. Fig. 2(c) shows that an increase in the aspect ratio increases the linearity at the expense of gauge factors. In the series of simulations, we adjust the aspect ratio of nanowires while keeping the volume

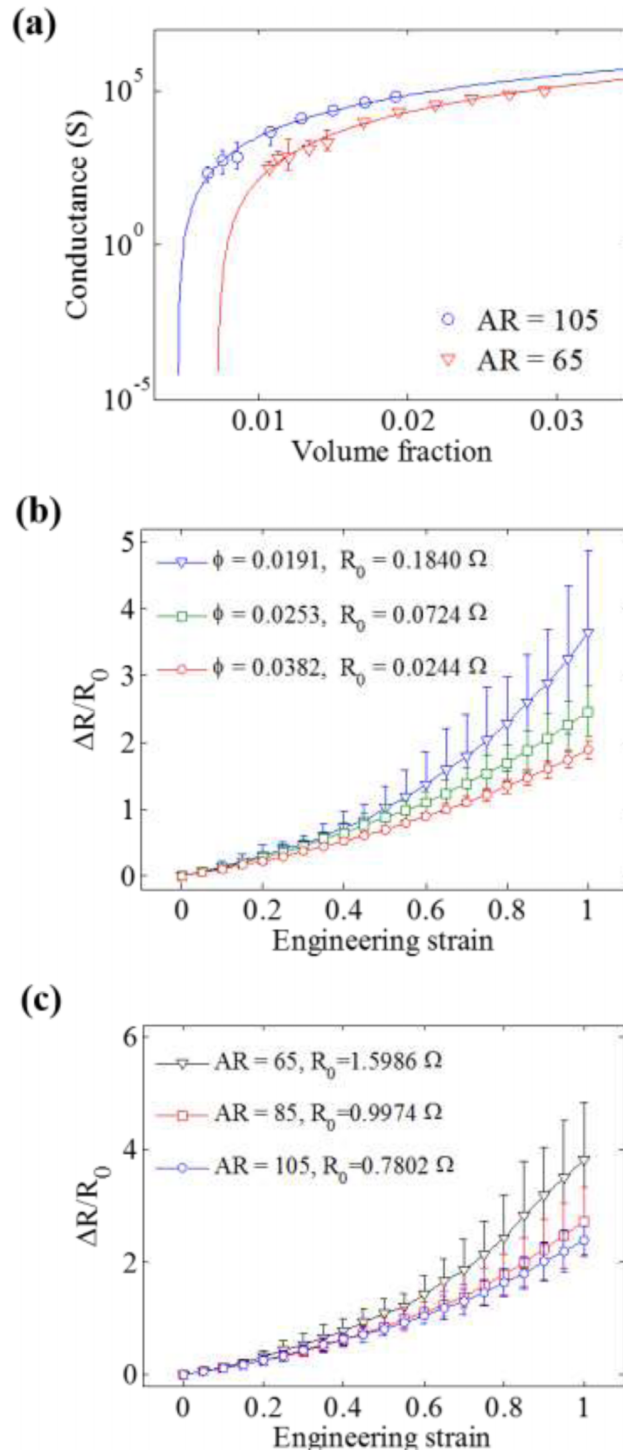


FIG. 2. (a) Comparison between the conductivities from simulations and percolation theory. (b) Resistance versus strain curves for different volume fractions when the diameter is 175 nm and the aspect ratio is 85. (c) Relative resistance change versus strain curves for various aspect ratios with the same volume fraction, 0.025.

fraction and nanowire diameter constant. Thus, number of nanowires are smaller for the simulation cells containing nanowires with higher aspect ratio. Whether the volume fraction or aspect ratio is controlled, simulation cells with lower initial resistance universally show better linear responses with lower gauge factors.

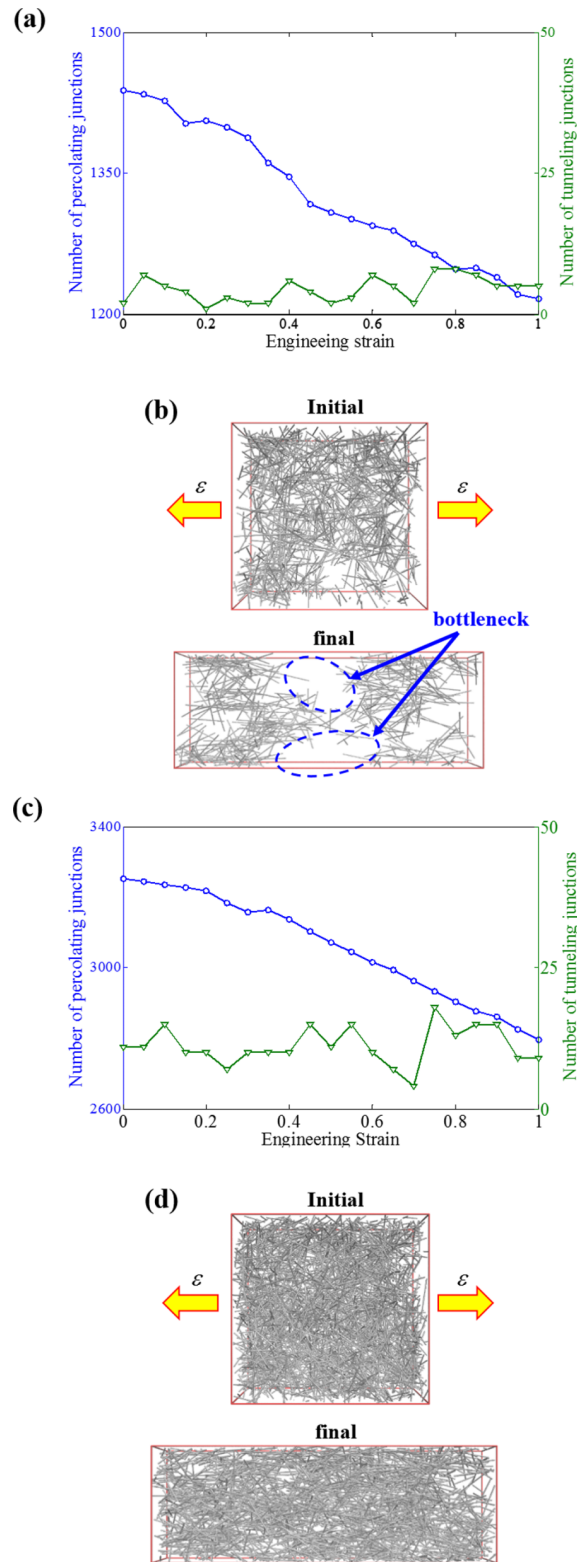


FIG. 3. The number of percolating junctions and tunneling junctions as a function of strain for the volume fraction of (a) 0.0125 and (c) 0.0191. The total number of nanowires are (a) 2214 and (c) 3260. Corresponding initial and final configurations of percolating nanowires are shown in (b) and (d), respectively. Identical size ($D=175\text{nm}$, $AR=85$) of nanowire is modelled for all cases. The snapshots were made from VMD 1.9.1.⁴⁰ The initial domain size for calculation is $([L_x, L_y, L_z]=[62.5\mu\text{m}, 60\mu\text{m}, 15\mu\text{m}])$.

We investigate the origin of nonlinear piezoresistivity at high strain, with results shown in Fig. 2(b)-2(c). The transition from low slope to high slope occurs earlier for lower volume fraction sensors, i.e. the linearity of the sensor worsens as the volume fraction decreases. For all the volume fractions we tested, the number of percolating nanowire junctions decreases almost linearly with applied strain, which does not explain the nonlinear behavior. The number of tunneling junctions is two orders of magnitude smaller than the number of completely connected junctions, and does not show any strong dependence on the strain. Instead, we find that the nonlinearity occurs when the network topology of a percolating cluster changes from homogeneous to inhomogeneous configuration with the emergence of a bottleneck in the electrical path (Fig. 3). The transition to

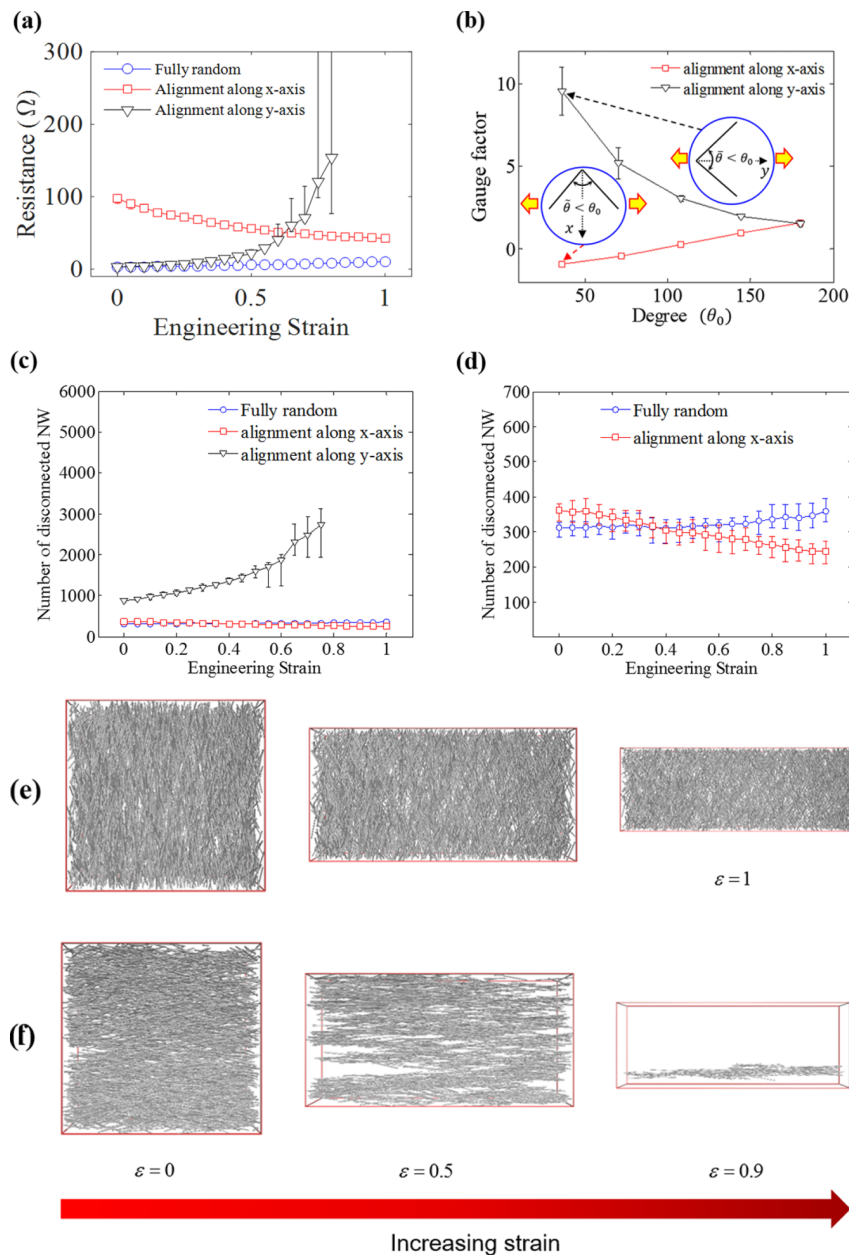


FIG. 4. (a) The piezoresistivity obtained for three different alignments. Also, specify the maximum allowable (b) The gradual change of gauge from negative to positive as a function of maximum allowable angles $\bar{\theta}$ and $\bar{\theta}$. The reduction of connected junctions is illustrated when the nanowires are aligned (c) along and (d) orthogonal to the tensile direction, with corresponding percolation network configurations in (e) and (f). The initial cell size is $([L_x, L_y, L_z] = [62.5\mu\text{m}, 60\mu\text{m}, 15\mu\text{m}])$.

inhomogeneous network occurs at higher strain for the denser nanowire network. A similar conclusion can be drawn from the change in the aspect ratio. At fixed volume fraction and fixed nanowire diameter, reduction in aspect ratio leads to an enhancement of the gauge factor, accompanied by a reduction of the linearity (Fig. 2(c)). In the previous work,²² we studied a thin slab geometry with no periodic condition along the z axis, and found the same mechanism for the nonlinear piezoresistive response. Thus, regardless of the details of the boundary conditions, the nonlinear piezoresistivity of the metal nanowire-elastomer nanocomposite with randomly oriented nanowires can be attributed to the topology change of the percolation network.

When the initial nanowire orientation is not random, an interesting piezoresistive response emerges that cannot be achieved by controlling the volume fraction or the aspect ratio, as depicted in Fig. 4(a)-4(b). As shown in the insets of Fig. 4(b), we can partially align the nanowires along the x axis (i.e. orthogonal to the tensile direction) by limiting the range of $\tilde{\theta}$ from 0 to θ_o where maximum angle θ_o is less than 180° . In a similar way, we can study the alignment along the tensile direction by limiting the $\tilde{\theta}$ range. Interestingly, when nanowires are strongly aligned to the x-axis, the resistance decreases with increasing strain, indicating a negative gauge factor (Fig. 4(a)-4(b)). In contrast, alignment along the tensile loading direction significantly increases the gauge factor. To summarize, without changing the aspect ratio or the volume fraction of the nanowires, the gauge factor can be tuned from negative to positive by changing the orientation distribution. Interestingly, this suggests that fabrication of a nanocomposite with zero gauge factor is feasible; such a nanocomposite could be utilized in highly stretchable electrodes for which minimum resistance change under tensile strain is desired.

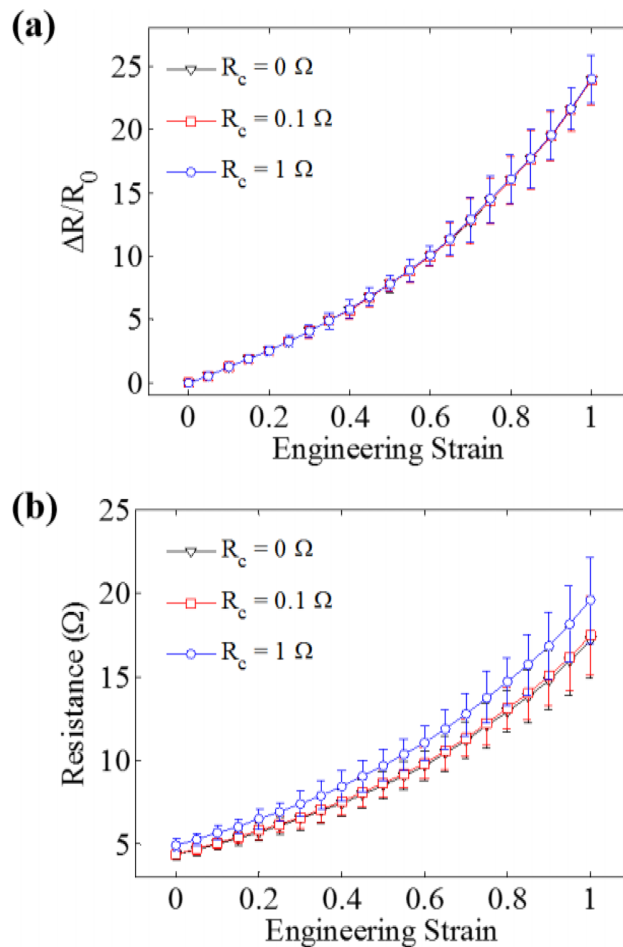


FIG. 5. (a) Absolute and (b) relative change of resistance as a function of strain with different contact resistances. Identical volume fraction (0.032) and initial configurations of nanowire (fully randomly oriented) are tested.

To the best of our knowledge, negative gauge factor has never been observed for metallic nanowire-elastomer nanocomposites. Negative gauge factor was reported for graphene ripple/PDMS nanocomposite based strain sensors, which has a completely different mechanism. The electron mobility of graphene increases when the wrinkles in a graphene sheet are flattened under tensile stretching, which results in the reduction of resistance.⁴⁵ We are pursuing the fabrication of strain sensors with varying nanowire orientations, which will be reported in our next paper.

In order to reveal the origin of orientation dependence, we analyzed the network connectivity change as a function of the strain, with results shown in Fig. 4(c)-4(d). When nanowires are strongly oriented along the x-axis with $\theta = 30^\circ$, the connectivity of the network increases as the strain increases, which is opposite to the case of a randomly oriented network. Stretching the nanocomposite leads to rotation of the nanowires toward the tensile loading direction; thus, the probability of making a connected junction increases (Fig. 4(e)).³⁸ On the contrary, when nanowires are aligned along the tensile direction, the junctions are quickly disconnected when the nanocomposite is stretched. Fig. 4(f) shows that the number of nanowires in the percolation network decreases with increasing strain. Therefore, the piezoresistivity of the nanowire-elastomer nanocomposites, regardless of the nanowire alignment and boundary conditions, can be attributed to the disconnection between adjacent nanowires, followed by percolation network topology change.

The aforementioned analyses are performed by assuming zero contact resistance between metal nanowires. The contact resistance between two silver rods is estimated to be in the range of 0.1 ohm to 1 ohm.⁴⁶ We perform simulations with two contact resistances of 0.1 ohm and 1 ohm for completely connected junctions. Fig. 5 shows that the contact resistance increases the absolute value of R, but the relative change, i.e. the gauge factor, is barely affected. Considering the relatively high modulus of the nanowires, we expect that the contact cross section as well as the contact resistance will not change significantly under tensile strain. Thus, while the contact resistance is assumed to be zero in piezoresistivity calculations, the mechanism revealed in this work will be valid in designing nanowire-elastomer nanocomposite based sensors.

CONCLUSIONS

We study the effects of volume fraction, aspect ratio, and alignment on the piezoresistive property of nanowire-elastomer nanocomposites. We find that the piezoresistivity of the nanowire-elastomer nanocomposites originates mainly from the disconnection of the inter-nanowire junctions in low strain regime, followed by the topology change of the percolation network in high strain regime. With decreasing volume fraction or aspect ratio, the gauge factor can be enhanced, while linearity is reduced. We also show that an anomalous negative gauge factor can be achieved when nanowires are aligned orthogonal to the loading direction. Our findings can serve as a guideline in designing nanowire-elastomer nanocomposite sensors with a wide range of gauge factor and stretchability.

ACKNOWLEDGEMENTS

This work was supported mainly by the Global Frontier Program (NRF-2008-2002807) and additionally by the Basic Science Research Program (2013R1A1A010091) of the National Research Foundation of Korea (NRF), funded by the Ministry of Science, ICT & Future Planning. N.M.P. is supported by the European Research Council (ERC StG Ideas 2011 BIHSNAM no. 279985 on ‘Bio-inspired hierarchical suprananomaterials’, ERC PoC 2013-1 REPLICA2 no. 619448 on ‘Large-area replication of biological anti-adhesive nanosurfaces’, ERC PoC 2013-2 KNOTTOUGH no. 632277 on ‘Super-tough knotted fibres’), by the European Commission under the Graphene Flagship (WP10 ‘Nanocomposites’, no. 604391) and by the Provincia Autonoma di Trento (‘Graphene nanocomposites’, no. S116/2012-242637 and reg. deliber. no. 2266).

¹ C. X. Liu and J. W. Choi, in *Conference proceedings : ... Annual International Conference of the IEEE Engineering in Medicine and Biology Society. IEEE Engineering in Medicine and Biology Society. Annual Conference 2009* (2009), pp. 6391-6394.

² I. Kang, M. J. Schulz, J. H. Kim, V. Shanov, and D. Shi, *Smart Materials and Structures* **15**(3), 737-748 (2006).

- ³ T. Yamada, Y. Hayamizu, Y. Yamamoto, Y. Yomogida, A. Izadi-Najafabadi, D. N. Futaba, and K. Hata, *Nat Nano* **6**(5), 296-301 (2011).
- ⁴ F. Lorussi, E. P. Scilingo, M. Tesconi, A. Tognetti, and D. De Rossi, *IEEE transactions on information technology in biomedicine : a publication of the IEEE Engineering in Medicine and Biology Society* **9**(3), 372-381 (2005).
- ⁵ T. Giorgino, P. Tormene, F. Lorussi, D. De Rossi, and S. Quaglioni, *IEEE transactions on neural systems and rehabilitation engineering : a publication of the IEEE Engineering in Medicine and Biology Society* **17**(4), 409-415 (2009).
- ⁶ X. Li, R. Zhang, W. Yu, K. Wang, J. Wei, D. Wu, A. Cao, Z. Li, Y. Cheng, Q. Zheng, R. S. Ruoff, and H. Zhu, *Scientific reports* **2**, 870 (2012).
- ⁷ M. Hempel, D. Nezhich, J. Kong, and M. Hofmann, *Nano letters* **12**(11), 5714-5718 (2012).
- ⁸ F. Xu and Y. Zhu, *Advanced materials* **24**(37), 5117-5122 (2012).
- ⁹ X. Xiao, L. Yuan, J. Zhong, T. Ding, Y. Liu, Z. Cai, Y. Rong, H. Han, J. Zhou, and Z. L. Wang, *Advanced materials* **23**(45), 5440-5444 (2011).
- ¹⁰ C. Cochrane, V. Koncar, M. Lewandowski, and C. Dufour, *Sensors* **7**(4), 473-492 (2007).
- ¹¹ D. Lee, H. P. Hong, M. J. Lee, C. W. Park, and N. K. Min, *Sensors and Actuators A: Physical* **180**, 120-126 (2012).
- ¹² M. H. Al-Saleh, G. A. Gelves, and U. Sundararaj, *Composites Part A: Applied Science and Manufacturing* **42**(1), 92-97 (2011).
- ¹³ E. Thommerel, J. C. Valmalette, J. Musso, S. Villain, J. R. Gavarrri, and D. Spada, *Materials Science and Engineering: A* **328**(1-2), 67-79 (2002).
- ¹⁴ C. Li and T.-W. Chou, *Composites Science and Technology* **68**(15-16), 3373-3379 (2008).
- ¹⁵ Y. Miao, Q. Yang, L. Chen, R. Sammynaiken, and W. J. Zhang, *Applied Physics Letters* **101**(6), 063120 (2012).
- ¹⁶ N. Hu, Y. Karube, M. Arai, T. Watanabe, C. Yan, Y. Li, Y. Liu, and H. Fukunaga, *Carbon* **48**(3), 680-687 (2010).
- ¹⁷ D. J. Lipomi, M. Vosgueritchian, B. C. Tee, S. L. Hellstrom, J. A. Lee, C. H. Fox, and Z. Bao, *Nature nanotechnology* **6**(12), 788-792 (2011).
- ¹⁸ S. Yun, X. Niu, Z. Yu, W. Hu, P. Brochu, and Q. Pei, *Advanced materials* **24**(10), 1321-1327 (2012).
- ¹⁹ P. Lee, J. Lee, H. Lee, J. Yeo, S. Hong, K. H. Nam, D. Lee, S. S. Lee, and S. H. Ko, *Advanced materials* **24**(25), 3326-3332 (2012).
- ²⁰ S. Han, S. Hong, J. Ham, J. Yeo, J. Lee, B. Kang, P. Lee, J. Kwon, S. S. Lee, M. Y. Yang, and S. H. Ko, *Advanced materials* **26**(33), 5808-5814 (2014).
- ²¹ P. Lee, J. Ham, J. Lee, S. Hong, S. Han, Y. D. Suh, S. E. Lee, J. Yeo, S. S. Lee, D. Lee, and S. H. Ko, *Advanced Functional Materials* **24**(36), 5671-5678 (2014).
- ²² M. Amjadi, A. Pichitpajongkit, S. Lee, S. Ryu, and I. Park, *ACS Nano* **8**(5), 5154-5163 (2014).
- ²³ C. Yang, H. Gu, W. Lin, M. M. Yuen, C. P. Wong, M. Xiong, and B. Gao, *Advanced materials* **23**(27), 3052-3056 (2011).
- ²⁴ H. Eom, J. Lee, A. Pichitpajongkit, M. Amjadi, J. H. Jeong, E. Lee, J. Y. Lee, and I. Park, *Small* **10**(20), 4171-4181 (2014).
- ²⁵ C. K. Jeong, J. Lee, S. Han, J. Ryu, G. T. Hwang, D. Y. Park, J. H. Park, S. S. Lee, M. Byun, S. H. Ko, and K. J. Lee, *Advanced materials* **27**(18), 2866-2875 (2015).
- ²⁶ K. K. Kim, S. Hong, H. M. Cho, J. Lee, Y. D. Suh, J. Ham, and S. H. Ko, *Nano letters* **15**(8), 5240-5247 (2015).
- ²⁷ S. Yao and Y. Zhu, *Nanoscale* **6**(4), 2345-2352 (2014).
- ²⁸ I. Chang, T. Park, J. Lee, H. B. Lee, S. Ji, M. H. Lee, S. H. Ko, and S. W. Cha, *International Journal of Hydrogen Energy* **39**(14), 7422-7427 (2014).
- ²⁹ I. Chang, T. Park, J. Lee, M. H. Lee, S. H. Ko, and S. W. Cha, *Journal of Materials Chemistry A* **1**(30), 8541-8546 (2013).
- ³⁰ T. Kim, Y. W. Kim, H. S. Lee, H. Kim, W. S. Yang, and K. S. Suh, *Advanced Functional Materials* **23**(10), 1250-1255 (2013).
- ³¹ D. Kim, L. Zhu, D.-J. Jeong, K. Chun, Y.-Y. Bang, S.-R. Kim, J.-H. Kim, and S.-K. Oh, *Carbon* **63**, 530-536 (2013).
- ³² S. Hong, H. Lee, J. Lee, J. Kwon, S. Han, Y. D. Suh, H. Cho, J. Shin, J. Yeo, and S. H. Ko, *Advanced materials* **27**(32), 4744-4751 (2015).
- ³³ X. Li, H. Gao, C. J. Murphy, and K. K. Caswell, *Nano letters* **3**(11), 1495-1498 (2003).
- ³⁴ C.-L. Wu, H.-C. Lin, J.-S. Hsu, M.-C. Yip, and W. Fang, *Thin Solid Films* **517**(17), 4895-4901 (2009).
- ³⁵ N. Hu, Y. Karube, C. Yan, Z. Masuda, and H. Fukunaga, *Acta Materialia* **56**(13), 2929-2936 (2008).
- ³⁶ Y. Zhu, Q. Qin, F. Xu, F. Fan, Y. Ding, T. Zhang, B. J. Wiley, and Z. L. Wang, *Physical Review B* **85**(4), 045443 (2012).
- ³⁷ J. G. Simmons, *Journal of Applied Physics* **34**(6), 1793-1803 (1963).
- ³⁸ M. Taya, W. J. Kim, and K. Ono, *Mechanics of Materials* **28**(1-4), 53-59 (1998).
- ³⁹ A. L. R. Bug, S. A. Safran, and I. Webman, *Physical Review Letters* **54**(13), 1412-1415 (1985).
- ⁴⁰ A. L. R. Bug, S. A. Safran, and I. Webman, *Physical Review B* **33**(7), 4716-4724 (1986).
- ⁴¹ I. Balberg, C. H. Anderson, S. Alexander, and N. Wagner, *Physical Review B* **30**(7), 3933-3943 (1984).
- ⁴² I. Balberg, N. Binenbaum, and N. Wagner, *Physical Review Letters* **52**(17), 1465-1468 (1984).
- ⁴³ S. I. White, R. M. Mutiso, P. M. Vora, D. Jahnke, S. Hsu, J. M. Kikkawa, J. Li, J. E. Fischer, and K. I. Winey, *Advanced Functional Materials* **20**(16), 2709-2716 (2010).
- ⁴⁴ S. Vionnet-Menot, C. Grimaldi, T. Maeder, S. Strässler, and P. Ryser, *Physical Review B* **71**(6), (2005).
- ⁴⁵ C. Wang, Y. Liu, L. Lan, and H. Tan, *Nanoscale* **5**(10), 4454-4461 (2013).
- ⁴⁶ S. Bin and J. Qu, presented at the Advanced Packaging Materials: Processes, Properties and Interfaces, 2005. Proceedings. International Symposium on, 2005 (unpublished).